# Combined Levitation Design and Control of a Novel M-DOF Actuator based on Air Bearing and Electromagnetic Principle

Zheng Li[1]
[1]*School of Electrical Engineering and Information Science, Hebei University of Science and Technology,*
*Yuhua East Road, 70#, Shijiazhuang 050018, P. R. China, phone: +86 311 86924334*
*lzhfgd@163.com*

***Abstract*—Supporting and levitation control are important for actuators or motors with complicated structures. Based on the presented configuration design, the simplified torque calculation model and non-linear system dynamic model have been proposed, and air bearing combined with magnetic levitation mechanism is developed for alleviating the friction and resistance to improve the dynamic performance of this M-DOF actuator. The fluid field model is built in computational fluid dynamics software. Different structure parameters and conditions are computed and compared with the vortex torque characteristics and pressure distribution. A linear mathematical model of the magnetic levitation force is deduced and corresponding control scheme with power drive unit is discussed. Experiment results show that the actuator can effectively implement 3-DOF motion combined with the combined levitation modes, and that the proposed approach can be applied to m-DOF actuators of the same kind effectively.**

***Index Terms*—Air bearing, magnetic levitation, M-DOF, actuators.**

## I. INTRODUCTION

With the development of the industry and technology, robot and manipulators which can achieve three-degree-of-freedom (3-DOF) motion are used more and more widely. This kind of devices are usually built with several convention driver motor, each having single degree-of-freedom, which reduces the position accuracy, efficient, dynamic performance of the system. In this condition, the multi-DOF actuators or motors have attracted many attentions [1]–[10]. To realize precision control, the feedback control system is necessary. However, the support mechanism design with measurement systems used for single-DOF feedback control system is not suitable for the multi-DOF feedback control system. So the bearing design and control becomes a crucial problem and should be paid more attentions. There are mainly four methodologies to support the multi-DOF rotor recently. These methods are classified into two kinds of contact and noncontact methods. Because of the flaws of contact measurement method, using non-contract method is the development trends of the bearing design. In the design of PM spherical actuator structure, the supporting structure is very important. According to the original content, design and analysis of the actuator structure, due to the actuator's unique three-dimensional spherical structure, making the use of contact ball bearing, the implementation is not entirely suitable for full rotation speed range and non-contact feature can be applied to complex three-dimensional structure of the bearing and lubrication. This paper mainly presents the application of combined air bearing and magnetic levitation for supporting the m-DOF rotor with satisfied performance.

Manuscript received March 20, 2012; accepted May 17, 2012.
This work was supported by the National Natural Science Foundation of China (under Grant No. 51107031, 50677013), the Natural Science Foundation of Hebei Province of China (under Grant No.E2009000703), the Foundation of Hebei Educational Committee (under Grant No.Z2010135), the Scientific Research Start Foundation of Doctoral Scholars of Hebei University of Science and Technology (under Grant No.QD200909) and the Funds for Distinguished Young Scholar of Hebei University of Science and Technology.

## II. OPERATION PRINCIPLE AND DYNAMIC ANALYSIS OF M-DOF PM ACTUATOR

The motor prototype consists of a ball-shaped rotor with four layers of 40 poles and two layers of 24 poles. There are10 poles with equally spaced position of alternative N-S distribution for the rotor. There are 12 poles in each layer and controlled separately for the stator. Fig. 1 shows the basic structure of the actuator. The actuator is designed to implement maximum 67 degrees tilt motion and 360 degrees rotation.

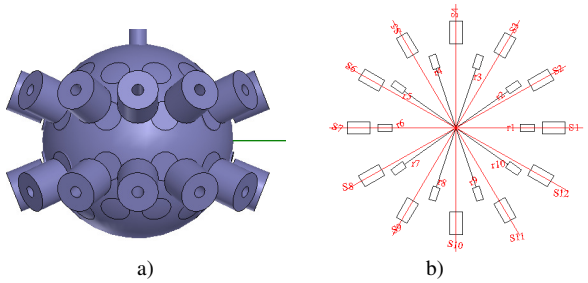

a) b)

Fig. 1. Basic structure of the actuator.

Using the Lagrange energy method, the dynamic equations of multi-DOF actuator are obtained. Each equation represents an axis of Cardian Angle. It can be seen that there

are many one-order and two-order coupling terms in the equation, which indicates serious inter-axes nonlinear coupling of the spherical actuator.

Like the conventional reluctance motors, the operation of the actuator is also based on the reluctance forces. The difference is that the flux path is not closed due to the non-magnetic material used in the rotor. It can be considered that the torque or force exerted on the rotor is the summation of individual rotor/stator pair interactions and the torque calculation model has the linear property.

The torque equation can be combined into one vector equation in the x-y-z coordinate [11]–[14]

$$\mathbf{T} = \frac{1}{2}\sum_{j=1}^{n_r}\sum_{k=1}^{n_s}\frac{\partial \Lambda_{jk}}{\partial \delta_{jk}} F_{jk}^2 \frac{\mathbf{r}_{rj}\times\mathbf{r}_{sk}}{\left\|\mathbf{r}_{rj}\times\mathbf{r}_{sk}\right\|}. \quad (1)$$

From (1), the torque calculation has been simplified to the superposition of torque component by individual pair as shown in Fig. 2. The former two parameters can be taken as torque constant, and derived by accurate computation or experiments. The torque produced by single stator/rotor pair can be written as

$$\mathbf{T_{jk}} = k(\delta_{jk}, i_k)\frac{\mathbf{r}_{rj}\times\mathbf{r}_{sk}}{\left\|\mathbf{r}_{rj}\times\mathbf{r}_{sk}\right\|} N i_j, \quad (2)$$

where the constant $k(\delta_{jk}, i_k) = \dfrac{\left\|\mathbf{T_{jk}}\right\|}{N i_j}$ is a function of $\delta_{jk}$ and $i_k$, so in the case of the reference torque is known, the control current corresponding to some rotor orientation can be solved by:

$$\mathbf{T} = \mathbf{K_T}\mathbf{I_d}, \quad (3)$$

$$\mathbf{I_d} = \mathbf{K_T}^{+}\mathbf{T}, \quad (4)$$

where $\mathbf{K_T}$ is the torque constant matrix about some orientation; $\mathbf{K_T}^{+}$ denotes its general inverse matrix. $\mathbf{I_d}$ is the reference control current.

By development and substitution, the complete mathematical model of the system can be written as

$$\mathbf{M(Q)}\ddot{\mathbf{Q}} + \mathbf{C(Q,\dot{Q})}\dot{\mathbf{Q}} + \mathbf{G(Q)} + \mathbf{T_{Qf}} = \mathbf{T_{Qe}}, \quad (5)$$

where:

$$\mathbf{M(Q)} = \mathbf{J_Q^T M_r J_Q} = \begin{pmatrix} J_{ba}c\beta^2 + J_b s\beta^2 & 0 & J_b s\beta \\ 0 & J_{ba} & 0 \\ J_b s\beta & 0 & J_b \end{pmatrix}, \quad (6)$$

$$\mathbf{C(Q,\dot{Q})} = \mathbf{J_Q^T M_r}\dot{\mathbf{J}}_\mathbf{Q} + \mathbf{J_Q^T C_r J_Q}, \quad (7)$$

$$\mathbf{G(Q)} = \mathbf{J_Q^T T_g} = m_c g r_c \begin{pmatrix} -s\alpha c\beta^2 c\gamma + s\beta c\beta s\gamma \\ -s\alpha c\beta s\gamma - s\beta c\gamma \\ 0 \end{pmatrix}, \quad (8)$$

$$\mathbf{T_{Qf}} = \mathbf{J_Q^T T_f}, \quad (9)$$

$$\mathbf{T_{Qe}} = \mathbf{J_Q^T T_e}. \quad (10)$$

The nonlinear friction has a great effect on the servo system and is hard to derive accurate mathematical models. Here, the design is performed by confirming its upper bound $\rho_f$, and was estimated by

$$\mathbf{T_{Qf}}(\dot{\mathbf{Q}}) = sign(\dot{\mathbf{Q}})\mathbf{T_c} + sign(\dot{\mathbf{Q}})(\mathbf{T_s} - \mathbf{T_c})\exp(-\mu\left|\ \dot{\mathbf{Q}}\ \right|), \quad (11)$$

where $\mathbf{T_s}$, $\mathbf{T_c}$, $\mu$ denote the static friction, coulomb friction and exponential constant.

The motor dynamics have the same form and properties as those of a robotic manipulator. The control scheme can be applied on the continuous trajectory tracking control, to minimize the effects of uncertainties including parameters perturbation, model error and outer disturbance.

## III. COMBINED LEVITATION SCHEME

In real applications, the air bearing and magnetic levitation principles are appropriate for the actuators with 3D structures. The air bear needs additional air source with large volume and relatively low control precision. The magnetic levitation usually performed with the decoupling of the electromagnetic system into torque and levitation sub-systems. However, the magnetic levitation is difficult to implement with large tilt angle of the rotor. So the most proper way for allevating the levitation problems is to combined with these 2 methods, using the air bearing as basic levitation mode especially for pan-tilt motions and the magnetic levitation mode for uniform spin rotation motion.

In the design of permanent magnet spherical actuator structure, the supporting structure is very important. According to the original content, design and analysis of the actuator structure, due to the actuator's unique three-dimensional spherical structure, making the use of hydraulic bearing, the implementation is not entirely suitable for gas bearing has a high flexibility and non-contact feature apply to complex three-dimensional structure of the bearing and lubrication. This project first application of air bearings in the motor of multiple degrees of freedom to explore and study.

The structure of the air bearing can be shown in Fig. 2. There is a gas film among the rotor spherical surface and the stator ball socket. When the pressure Ps gas through the orifice into the air film, the hole after the pressure dropped to Pd, the sphere is moving along the axis of symmetry, each orifice pressure is bound to each other are equal. Gas outflow from the orifice to the outer boundary of the θ2 cone to flow directly into the atmosphere. Gas pressure behind the orifice of Pd is gradually reduced to the boundary at ambient pressure Pa. Pd gradually become Pa pressure caused by the carrying capacity of the spherical bearing. Gas pressure in the horizontal projection of the sphere is symmetrical, so the horizontal force is zero, while in the vertical projection of oz axis to form a spherical bearing. From the floating amount h increases, the formation of the gas film thickness, so that the

air flow resistance is smaller, the increased traffic flow, so that through the orifice of the pressure drop increases, the outer Pd will be reduced to the same supply pressure Ps small, resulting in the total supporting force projection will also be smaller in the oz axis. On the contrary, became a floating minus hours and work together on the oz-axis projection will increase. When the ball bearing structure and the gas pressure is constant, since the float and carrying capacity is one to one.

For this study the flow of the ball bearings, do the following assumptions:

1) The lubrication gas is taken as a Newtonian fluid, gas viscosity coefficient μ is constant;
2) Gas membrane gas flow for the isothermal process, the boundary layer is fully developed laminar flow is stable;
3) Do not consider the impact of gravity on the gas;
4) Take the gas as an ideal gas.

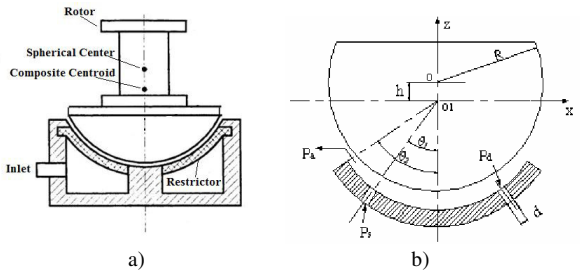


Fig. 2. Illustration of the static pressure spherical air bearing.

According to the assumptions, the control equation can be simplified to model calculations, based on the use of CFD software (the Fluent). This work uses CFD analysis software for the numerical calculation, so it is necessary to use pre-processing software for flow field modeling of flotation ball bearings, and mesh generation, mesh type, density, quality, and local processing of computational efficiency and accuracy. Aerostatic ball bearings the flow field numerical calculation, the gas film thickness of the thin (micron) and thickness and circumference size difference of thousands of times. Reduce the computational truncation errors, preventing calculation divergence meshing using hexahedral and pyramid grid. Around the expected pressure and speed of change is more intense for stomatal using structured hexahedral grids and local refinement. The volume mesh with air feed holes is shown in Fig. 3.

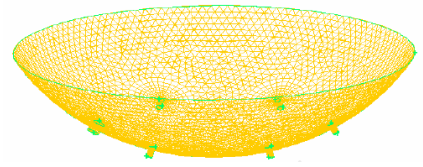

Fig. 3. Mesh of the volume with the air feed holes.

CFD analysis software can be 2D and 3D model calculation also provides a single-precision and double precision solver. In most cases, single-precision solver is efficient and accurate, but the slender pipe model and the gas lubrication model, the direction of length scales much difference, describing the coordinates of the nodes single-precision grid computing would be appropriate. Therefore, the project uses a 3D model of the double-precision solver.

CFD analysis software also provides a separation and coupling two solvers, two solutions are applicable to a wide range of pressure from incompressible to high-speed flow. When computing high-speed compressible flow, the coupled solver is with advantage of faster convergence. Coupled solver of memory needed is about 1.5 to 2 times the separation solver, in view of the gas lubrication problem in the gas flow rate and pressure are not very high, so the separate solver memory is chosen.

In the choice of viscosity model, the gas film thickness used in the model is quite small, and low gas pressure, gas flow rate is very slow, so I chose the laminar flow model, so that both meet the required precision, but the calculation is relatively low.

To the setting boundary conditions, they are only related to the pressure inlet (pressure-inlet) pressure outlet (pressure-outlet), the fixed wall (wall) and three boundary conditions. 6 for the boundary of the pores at the entrance is set to the pressure inlet boundary condition, the surface pressure and the absolute pressure, operating pressure have the following relations

$$P_{absolute} = P_{gauge} + P_{operating}\,. \tag{7}$$

In addition, the size of the surface pressure is the total pressure on the inlet boundary. On non-pressure flow

$$P_{total} = P_{static} + \frac{1}{2}\rho v^2. \tag{8}$$

For compressible flow

$$P_{total} = P_{static}\left(1+\frac{k-1}{2}Ma^2\right)^{k/(k-1)}. \tag{9}$$

For the pressure outlet boundary conditions, torus selected as the pressure outlet boundary, shown in Fig. 4. The CFD analysis software, up and down two goals of the gas film surface (surface 3, surface 4) set into a non-slip wall. Study of the air bearing gas flow diffusion faster and therefore do not consider the effect of a fixed wall heat transfer. From the above, the calculation of the air bearing of the actuator model can be derived.

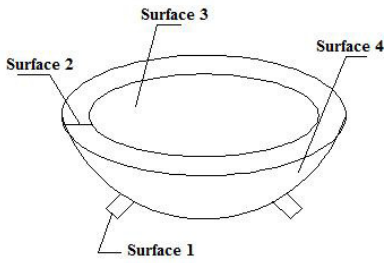


Fig. 4. Diagrammatic sketch for setting boundary conditions.

From the ball bearings in the standard model of the flow field pressure distribution map of Fig. 5, it can be clearly shown that on the wall of the pressure distribution of the flotation ball bearings is a symmetrical structure, so the pressure line of the gas membrane such as is almost space concentric circles, beginning from the 6 around the orifice to the pressure outlet boundary, the pressure value is constantly

decreasing pressure to the pressure outlet location approximate decay to zero. From the Fig. can also see the value in the 6 air feed holes, orifice pressure, and almost exactly the same.

In the case of change of the throttle position, to discuss the supply holes 1 and the angle between the vertical plane yo1z the impact of the vortex torque on the angle between the changes, and two supply holes as the following two situations described.

This article in the standard model will be between 25-35 degrees change in value, and calculate the eddy current torque value corresponding to the change, to map out the relationship with the vortex torque curve shown in Fig. 6.

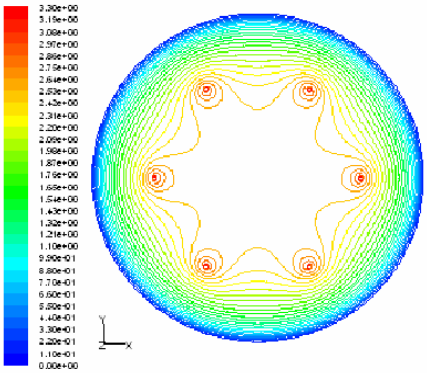

Fig. 5. Pressure distribution of standard cases.

In the standard model $\theta_1 = 30^o$, change $\theta_1$ from 25 to 35 degrees and the pressure distribution diagram can be shown as Fig. 7. It can be seen from the diagram that when (a) = 25 degrees, the hole 1 pressure around than the other five holes around the pressure has increased, caused the increase of bearing capacity; when $\theta_1$= 35 degrees, from the diagram (b) it can be seen that the surrounding pressure of hole 1 is decreased relative to the other five holes' pressure, caused the bearing capacity decline.

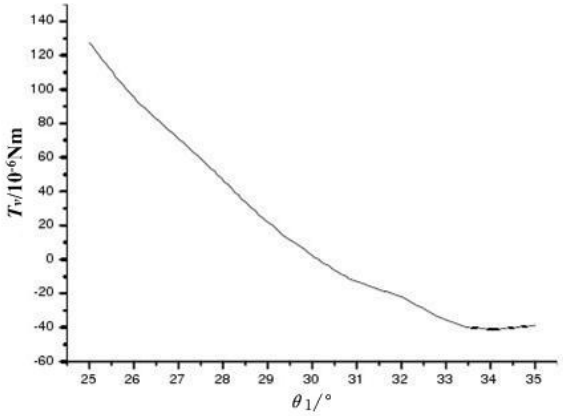


Fig. 6. Curve of relation between $\theta_1$ and vortex torque.

When the actuator perform slight pan-tilt motion, the joint activation of spin and tilt can be performed, so the main spin motion can be considered for adding magnetic levitation mechanism. Like common bearingless motors, the use of the original bias magnetic field and adding a magnetic field to achieve levitation to produce a controlled force to drive the actuator should be in the case that the pole pairs' number of magnetic field and levitation number must be a difference of ± 1. The principle of M-DOF actuator is slightly different for the levitation process of common bearingless motors. The levitation is limited as an auxiliary mode for only in spin motion and pan-tilt motion can be used as fine orientation adjustment.

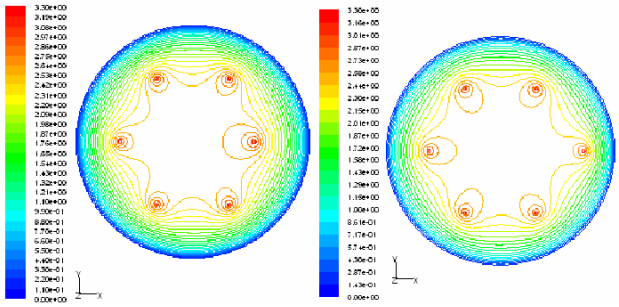

a) b)

Fig. 7. Pressure distribution of different $\theta_1$ : (a) $\theta_1$ =25°, (b) $\theta_1$ =35°

Actuator radial levitation force generation is of active levitation control. Usually the bearingless permanent magnet motor stator windings produce two default kinds of effects on the number of different magnetic poles, those poles producing the magnetic torque with *pt* number of pole pairs and the levitated magnetic force with *ps* number of pole pairs. The former and the same number of pole pairs of the rotor permanent magnet magnetic field pt produce drive torque for rotor rotation, while the presence of the latter is to break the balance of the original air-gap magnetic field resulting in levitation of the rotor by supporting radial levitation force. When the two kinds of magnetic field share the rotation direction, the same electrical angular frequency, and to meet *pt* = *ps* ± 1, the levitation force can be produced and controlled.

The permanent magnet actuator structure of one payer is shown in Fig. 8. The actuator is with magnetizing two pairs of radial surface mount permanent magnet poles as the rotor teeth centralized structure and the stator structure. As the rotor axial length of the sheet is much smaller than the diameter length, according to the known magnetic resistance characteristics: the rotor in the axial and torsional directions are passive suspension control, i.e. if there is tilt or axial rotor displacement, the role of magnetic resistance will make it back to its balanced position.

In the realization of this kind of structure, the stator current can be taken as including two components, producing the torque magnetic field and levitation magnetic field respectively with the name of stator current torque component and levitation component. So the currents in 12 coils on single layer can be expressed as

$$i_k = i_{tk} + i_{sk}, \tag{10}$$

where *k*=1,…,12; $i_k$ is the current in stator coil, $i_{tk}$, $i_{sk}$ are the torque and levitation component respectively.

Here the pole pair number of torque magnetic field is $p_t = 5$, the pole pair number of levitation magnetic field is $p_s = 1$. The stator current can be taken as superposition of

torque component $i_{tk}$ and levitation component $i_{sk}$.

The stator current levitation component can be written as

$$\begin{bmatrix} i_{s1} \\ i_{s2} \\ i_{s3} \\ i_{s4} \\ i_{s5} \\ i_{s6} \\ i_{s7} \\ i_{s8} \\ i_{s9} \\ i_{s10} \\ i_{s11} \\ i_{s12} \end{bmatrix} = i_{sd} \begin{bmatrix} \cos(\theta_s) \\ \cos(\theta_s - 30^\circ) \\ \cos(\theta_s - 60^\circ) \\ \cos(\theta_s - 90^\circ) \\ \cos(\theta_s - 120^\circ) \\ \cos(\theta_s - 150^\circ) \\ \cos(\theta_s - 180^\circ) \\ \cos(\theta_s - 210^\circ) \\ \cos(\theta_s - 240^\circ) \\ \cos(\theta_s - 270^\circ) \\ \cos(\theta_s - 300^\circ) \\ \cos(\theta_s - 330^\circ) \end{bmatrix} - i_{sq} \begin{bmatrix} \sin(\theta_s) \\ \sin(\theta_s - 30^\circ) \\ \sin(\theta_s - 60^\circ) \\ \sin(\theta_s - 90^\circ) \\ \sin(\theta_s - 120^\circ) \\ \sin(\theta_s - 150^\circ) \\ \sin(\theta_s - 180^\circ) \\ \sin(\theta_s - 210^\circ) \\ \sin(\theta_s - 240^\circ) \\ \sin(\theta_s - 270^\circ) \\ \sin(\theta_s - 300^\circ) \\ \sin(\theta_s - 330^\circ) \end{bmatrix}, \quad (11)$$

where $i_{sd}$ and $i_{sq}$ are the projection value of joint vector of stator current on the $dq$ frame; $\theta_s$ is the electric angle position with respect to the $dq$ frame.

In practice, the control law of $i_d = 0$ is adopted for magneto-force orientation, thus $i_{td} = 0$.

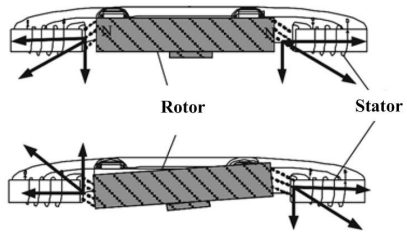


Fig. 8. Principle of the magnetic levitation.

According to magnetic circuit calculation, the relationship between the stator coil and the rotor permanent magnet can be expressed as [15]

$$F_k = \frac{(f_k + f_{rk})^2}{\mu_0 r d \alpha^2 R^2} \sin(\alpha_0 / 2), \quad (12)$$

where $k$ is the number of stator coil, $f_{rk}$ is the magneto-force of each magnetic circuit, $R$ is the air gap reluctance, $d$ is the axial direction length, $\alpha_0$ denotes the tooth radian angle of stator.

The 12 stator coils magnetic force exerted on the rotor can be decomposed to X and Y directions as the radial components of levitation force:

$$F_X = \sum_{k=1}^{12} F_k \cos[30^\circ (k-1)], \quad (13)$$

$$F_Y = \sum_{k=1}^{12} F_k \sin[30^\circ (k-1)]. \quad (14)$$

Using the levitation and torque model, the closed-loop rotor position control can be realized based on the radial displacement to derive the stator current levitation component. The torque component can be adjusted by the ordinary PI controller. From the schematic illustration as shown in Fig. 9, the stator currents can be calculated and adopted to control 12 stator coils by the power electronics system. The drive unit for each coil is chosen as H-bridge circuit respectively. The unit is integrated with IC and do not need to input detailed control signal for each switching device to control the magnitude and direction of currents for reducing the workload. The displacements' PID, rotation speed' PI, torque and levitation force calculation are completed by DSP controller without additional analog circuit built.

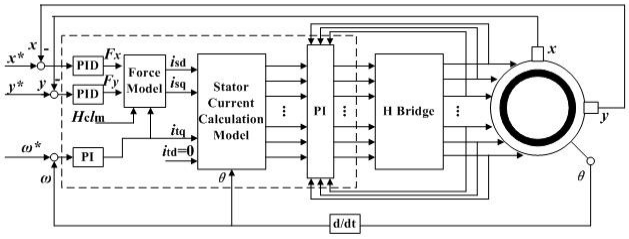


Fig. 9. Illustration of basic control blocks.

## IV. EXPERIMENTAL RESULTS

To validate the performance of the levitation system, experiments are carried out. Manufactured experiment prototype can be shown in Fig. 10. The length of output shaft is designed to 55mm and the angle resolution for three degree-of-freedom can averagely reach to 1 degree, which can meet the demands for most applications. The measured results of radial position of the rotor can be shown in Fig. 11 and Fig. 12.

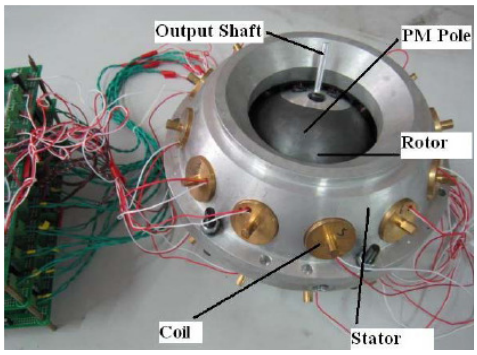


Fig. 10. Experiment prototype of M-DOF actuator.

The spin rotation movement is in static and dynamic state and the displacements are measured by eddy currents sensor with relative 0.1 $\mu$m accuracy. The eddy current sensor is used as the fine displacement measurement system. Theoretically a total of three layers of eddy current sensors can be placed between the stator and rotor, including placed on the two layers of stator magnetic poles' center position and one layer placed in the equatorial plane, however, in the experiment only 2 sensors are placed on each layer to measure the air gap with 3 planes. For the multi-DOF space motion measurement with respect to the initial position, the three Euler angles are able to be obtained from the CCD-based non-contact detection system with satisfied accuracy as used in [11]. From Fig. 11, it can be seen the rotor's

position is limited in 150 $\mu$m in steady levitation state and 60 $\mu$m in dynamic levitation state in light load conditions. The errors have been controlled within satisfied range, with the presented control scheme. The air bearing can effectively improve the stability of magnetic levitation and extend the range of levitation motion.

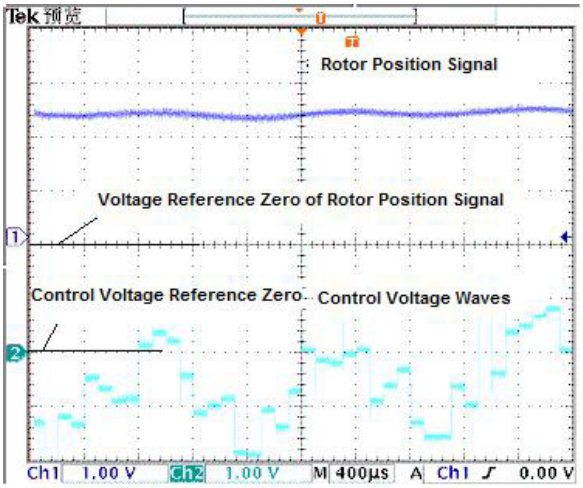


Fig. 11. Measured waves of static levitation process.

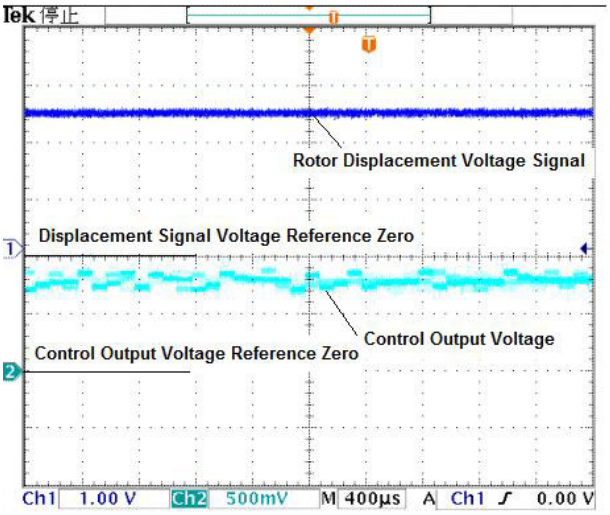


Fig. 12. Measured waves of dynamic levitation process.

## V. CONCLUSIONS

This paper presents the combined air bearing and magnetic levitation methodology for multi-DOF actuator or motor applications. The two methods are all applied in related industrial areas with their special features of advantages. In this work, the air bearing is used for basic supporting and pan-tilt motion with relatively large amplitude; the magnetic levitation mainly used for spin rotation and slightly pan-tilt motions. Experiment is carried out to validate the effectiveness of presented methodologies by setting a motion in sequence. The results prove the methodology is available and effective. It is expected that the presented scheme is able to provide a reference for further research and investigation for similar measurement problems of multi-DOF actuators or motors.

## REFERENCES

[1] G. S Chirikjian, D. Stein, "Kinematic design and commutation of a spherical stepper motor", *IEEE Trans. on Mechatronics,* vol. 4, no.4. pp. 342–353, 1998. [Online]. Available: http://dx.doi.org/10.1109/3516.809513

[2] D. Stein, G. S. Chirikjian, "Experiments in the Commutation and Motion Planning of a Spherical Stepper Motor", in *Proc. of the ASME Design Engineering Technical Conferences and Computers and Information in Engineering Conference,* 2000, pp. 1–7.

[3] K. Davey, G. Vachtsevanos, R. Powers, "The analysis of fields and torques in spherical induction motors", *IEEE Trans. on Magnetics, v*ol. 23, no. 1, pp. 273–282, 1987. [Online]. Available: http://dx.doi.org/10.1109/TMAG.1987.1064749

[4] A. Raye, Lee Kok-Meng, "Finite Element Torque Modeling for the Design of a Spherical Motor", in *Proc. of the 7th Int. Conf. on Control, Automation and Robotics and Vision*, 2002, pp. 390–395.

[5] J. Wang, G. W. Jewell, D. Howe, "Analysis, design and control of a novel spherical permanent-magnet actuator", *IEE Electric Power Applications*, vol. 145, no. 1, pp. 61–71, 1998. [Online]. Available: http://dx.doi.org/10.1049/ip-epa:19981635

[6] B. Dehez, G. Galary, D. Grenier, et al., "Development of a Spherical Induction Motor With Two Degrees of Freedom", *IEEE Trans. on Magnetics*, vol. 42, no. 8, pp. 2077–2089, 2006. [Online]. Available: http://dx.doi.org/10.1109/TMAG.2006.876473

[7] Qunjing Wang, Zheng Li, Youyuan Ni, et al., "Magnetic Field Computation of a PM Spherical Stepper Motor Using Integral Equation Method", *IEEE Trans. on Magnetics,* vol. 42, no. 4, pp. 731–734, 2006. [Online]. Available: http://dx.doi.org/10.1109/TMAG.2006.871399

[8] Zheng Li, Yongtao Wang, "Finite Element Analysis and Structural Optimization of a Permanent Magnet Spherical Actuator", *Elektronika ir Elektrotechnika (Electronics and Electrical Engineering*), no. 8, pp. 67–72, 2011.

[9] A. Petridis, A. Bakirrzis, "Varying Fitness Function in Genetic Algorithm Constrained Optimization: The Cutting Stock and Unit Commitment Problem", *IEEE Trans. on System Man and Cybernetics*, vol. 28, no. 5, pp. 629–640, 1998. [Online]. Available: http://dx.doi.org/10.1109/3477.718514

[10] Zhe Qian, Qunjing Wang, Lufeng Ju, Anbang Wang, et al., "Studies on vision based absolute orientation detection method of spherical motor", in *Proc. of the International Conference on Electrical Machines and Systems*, 2009, pp. 1–6.

[11] A.Grainys, J. Novickij, "The Investigation of 3D Magnetic Field Distribution in Multilayer", *Elektronika ir Elektrotechnika (Electronics and Electrical Engineering*), no. 7, pp. 9–12, 2010.

[12] Wang Qunjing, Li Zheng, Xia Kun, et al., "Calculation and Analysis on Configuration Parameters and Torque Characteristics of a Novel Spherical Stepper Motor", in *Proc. of the CSEE*, 2006, pp. 158–165.

[13] Zheng Li, Qunjing Wang, "Modeling and Control of a Permanent Magnet Spherical Stepper Motor", in *Proc. of the International Conference on Electrical Machines and Systems*, 2007, pp. 1574–1579.

[14] Zheng Li, "Robust control of PM spherical stepper motor based on neural networks", *IEEE Trans. on Industrial Electronics*, vol. 56, no. 8, pp. 2945–2954, 2009. [Online]. Available: http://dx.doi.org/10.1109/TIE.2009.2023639